IEEE Access
Multidisciplinary | Rapid Review | Open Access Journal

Received July 31, 2019, accepted August 18, 2019, date of publication August 22, 2019, date of current version September 5, 2019.

Digital Object Identifier 10.1109/ACCESS.2019.2936949

Sparsity-Based Direction-of-Departure and Direction-of-Arrival Estimation for Bistatic Multiple-Input Multiple-Output Radar

QIANPENG XIE[1], XIAOYI PAN[1], MIN HUANG[2], JIYUAN CHEN[1], AND SHUNPING XIAO[1]

[1]State Key Laboratory Complex Electromagnetic Environment Effects on Electronics and Information System, National University of Defense Technology, Changsha 410073, China

[2]College of Information Engineering, Shenzhen University, Shenzhen 518061, China

Corresponding author: Xiaoyi Pan (pan_xiao_yi@hotmail.com)

This work was supported in part by the National Natural Science Foundation of China under Grant 61701507, Grant 61890542, and Grant 61571451.

ABSTRACT This paper provides an efficient method to determine the direction of departure (DOD) and direction of arrival (DOA) in bistatic multiple-input multiple-output (MIMO) radars. The proposed method firstly decouples the DOD and DOA parameters by converting the original received signal model into two separate new signal models. The new signal model corresponding to DOA can be directly obtained by matched filtering operation. In order to obtain the model for DOD, vectorization operation and kronecker transformation are utilized after the matched filtering operation. Both the new signal models for DOA and DOD behave like an augmented signal model of uniform linear array (ULA). Then, a covariance- vector sparsity-aware estimator is developed to find the accurate angular parameter. Meanwhile, in order to improve the estimation accuracy, the additive noise is eliminated by exploiting the toeplitze structure inherent in the array received covariance matrix and the asymptotic distribution of the sampling errors is also derived. Furthermore, the regularization parameter setting used by the proposed estimator is derived with the aid of the Lagrangian duality theory to guarantee the sparsity of solution. Simulation results are conducted to verify the effectiveness and the superiority of the sparsity-based estimator over other methods in terms of the angular estimation accuracy.

INDEX TERMS Bistatic MIMO radar, DOD estimation, DOA estimation, sparsity-aware estimator.

I. INTRODUCTION

In recent years, the estimation of angular parameters in multiple- input multiple-output (MIMO) radar has become a hot research topic [1]–[4] due to its advantages in the field of radar signal processing. MIMO radar together with orthogonal waveforms can obtain higher resolution, better parameter identifiability, greater flexibility in the beampattern design and more degrees of freedom (DOFs) over the conventional phased-array radar associated with coherent waveforms [5]–[7]. According to [8] and [9], MIMO radar systems are generally categorised into the statistical MIMO radar systems and the colocated MIMO radar systems. Furthermore, the colocated MIMO radars can be divided into bistatic and monostatic MIMO radars. In bistatic MIMO radars, the direction-of-departure (DOD) and direction-of-arrival (DOA) are totally different due to the transmit array and receive array are separated away from each other, while the DOD and DOA can be regarded as the same because the transmitters and receivers are close enough.

In order to determine the DOD and DOA estimation in bistatic MIMO radars, a number of effective methods have been proposed. In [10] and [11], a two-dimensional (2D) Capon estimator and 2D MUSIC estimator are proposed to estimate the DOD and DOA by using a 2D peak search process at the cost of high computational complexity. In order to reduce the computational load, the corresponding reduced-dimensional Capon (RD-Capon) [12] and RD-MUSIC [11] algorithms are conducted to identify the DOD and DOA. Furthermore, in order to avoid peak searching, the estimation of signal parameters via rotational invariance technique (ESPRIT) is tailored to determine the angular parameter in bistatic MIMO radars [13] and [14]. The polynomial root finding algorithm with automatical angular pairing is proposed in [15] for jointly estimating of DOD and DOA. In [16], a method combining the ESPRIT and SVD of

The associate editor coordinating the review of this article and approving it for publication was Nosherwan Shoaib.

cross-correlation matrix is put forward to obtain the closed-form solution for angular parameter estimation in bistatic MIMO radars. In [17], an alternating-projection-based maximum likelihood (ML) estimators is presented to enhance the DOD and DOA estimation performance even when the impinging targets are coherent. In [18], an ESPRIT-like estimator and a maximum likelihood estimator are proposed to determine more targets than the number of physical sensors under the condition of Swerling-II targets. Compared with Swerling-I targets, the method in [18] can identify four times targets. In [19], [20], the joint diagonalization method is devised to increase the degrees of freedom (DOFs) both for ULA and L-shaped transmit and receive array structures in bistatic MIMO radar system. In [21]–[23], in order to exploit the multidimensional structure inherence in the bistatic MIMO radar data, the third-order tensor-based methods are proposed to estimate the DOD and DOA after matched filtering operation. Besides, matrix completion as a significant mathematics tool is employed for target localization in bistatic MIMO radar when there exist missing entries in the collected data after the matched filtering [23]. Nevertheless, the resolution and accuracy of the aforementioned approaches to DOA and DOD joint estimation for MIMO radar will degrade in low signal-to-noise ratio (SNR) region and/or small sample situation. As a matter of fact, the sparse structure inherent in the radar data has not yet been employed by the aforementioned methodologies, which, when appropriately utilized, is able to significantly enhance the resolution as well as accuracy in DOA and DOD estimation.

It has been demonstrated that the sparsity-based methods in angular parameter estimation have attracted great interests due to theirs high resolution in the case of low SNR and limited snapshots [24]–[29]. In [24], [25], the reweighted ℓ_0-norm and ℓ_1-norm sparse representation methods are proposed to improve the DOA estimation accuracy for monostatic MIMO radars. In [26], a nuclear norm minimization (NNM) algorithm based on the noncircular property of the signals is adopted to extend the array aperture in monostatic MIMO radars. In [27], in order to deal with the unknown mutual coupling problem in monostatic MIMO radars, the sparse method for direction finding has been suggested based on the second order statistics and fourth-order cumulants. In [29], a real-valued sparse Bayesian learning algorithm is derived to deal with the DOA estimation for monostatic MIMO radar under the condition of unknown nonuniform noise. However, the aforementioned sparsity-based methods only focus on improving the estimation performance in monostatic MIMO radar. Unlike the monostatic MIMO radar, the DOD and DOA in bistatic MIMO radar are different, causing more angular parameters to be estimated. Therefore, it is nontrivial to reformulate the sparse direction finding approach for the bistastic MIMO radar. Furthermore, the dictionary matrix becomes huge in size if the whole 2D detection area is discretized. The design issue of large-scale dictionary matrix for the 2D direction finding turn out to be ill-conditioned, which has not yet been addressed in the literature. In order to apply the sparsity-based methods to the bistastic MIMO radar successfully, a special sparsity-aware estimator is proposed. It is revealed that the devised sparse recovery algorithm is able to avoid discretizing the whole 2D detection area and significantly enhance the DOD and DOA estimation performance in the low SNR and small samples environment.

To summarize, the main contributions of this work can be given as follows:

- Two new signal model for DOD and DOA are constructed, which can be able to decouple the DOD and DOA parameters. This in turn allows us to separately determine DOD and DOA parameters.
- A sparse representation estimator for direction finding is devised, which is able to efficiently employ the sparse structure inherent in the array covariance matrix, leading to accurate direction finding for bistatic MIMO radar. To further improve the estimation performanace, a selection matrix to eliminate the background noise and a whitening filter to suppress the residual error are also suggested.
- In order to guarantee the sparsity of the solution, the regularization parameter selection in the proposed sparse recovery model is correctly determined by using the Lagrangian duality theory.

The rest of this paper is organized as follows. In Section II, data model is addressed. In Section III, we describe the proposed covariance sparsity-aware algorithm for DOD and DOA estimation. In Section IV, the performance of the proposed method is evaluated through extensive simulations and Section V concludes the paper.

Notations: Throughout this paper, scalars, vectors and matrices are denoted by lowercase letters, boldface lowercase letters and boldface uppercase letters, respectively. The superscripts $*$, T and H denote the complex conjugate, the transpose, and the complex conjugate transpose, respectively. The Moore-Penrose pseudoinverse is denoted by the superscript $\dagger$ and $\mathbb{E}(\cdot)$ represent the expectation operation. The symbol $\otimes$ and $\odot$ denote the Kronecker product and Kronecker-Rao operation, respectively. The $vec(\mathbf{A})$ denotes vectorization, which converts a matrix into a column vector by stacking the columns of the matrix on top of one another. Additionally, $\mathbf{0}$ and $\mathbf{I}$ denote the zero matrix and identity matrix with appropriate dimensions.

II. SIGNAL MODEL

Consider a bistatic MIMO radar system equipped with M transmit arrays and N receive arrays to locate K targets in the two-dimension detection area. Both arrays are omnidirectional ULAs with half-wavelength element spacing. At the transmit array, M elements are used to emit orthogonal narrowband waveforms with identical bandwidth and center frequency. And, assume that the reflection dopper frequencies have no effect on the orthogonality between the transmitted and received waveforms. The transmit orthogonal waveform

can be denoted as $\boldsymbol{S} = [\boldsymbol{s}_1, \boldsymbol{s}_2, \cdots, \boldsymbol{s}_M]^T \in \mathbb{C}^{M\times P}$, where P is the number of samples per pulse period. Assume that there are K narrowband far-field uncorrelated targets located in the same range bin of interest with $(\alpha_k, \beta_k), k = 1, 2, \cdots, K$, where α_k and β_k denotes the DOD and DOA of the k-th target. Thus, the signal model at the receiver can be expressed as

$$\boldsymbol{X} = \sum_{k=1}^{K} \gamma_k \boldsymbol{b}(\beta_k)\boldsymbol{a}^T(\alpha_k)\boldsymbol{S} + \boldsymbol{W} \tag{1}$$

where γ_k denotes the reflection coefficients of K targets, $\boldsymbol{b}(\beta_k) = [1, e^{j\pi \sin(\beta_k)}, \cdots, e^{j\pi(N-1)\sin(\beta_k)}]^T \in \mathbb{C}^{N\times 1}$ is the steering vector corresponding to DOA and $\boldsymbol{a}(\alpha_k) = [1, e^{j\pi \sin(\alpha_k)}, \cdots, e^{j\pi(M-1)\sin(\alpha_k)}]^T \in \mathbb{C}^{M\times 1}$ is the steering vector corresponding to DOD. $\boldsymbol{W}$ denotes the additive Gaussian white noise. Due to the orthogonality between the transmit and receive waveforms, the output data at the receive array after the matched filtering operation with $\boldsymbol{S}^H$ can be expressed as

$$\begin{aligned}\bar{\boldsymbol{X}} &= \sum_{k=1}^{K} \gamma_k \boldsymbol{b}(\beta_k)\boldsymbol{a}^T(\alpha_k)\boldsymbol{S}\boldsymbol{S}^H + \boldsymbol{W}\boldsymbol{S}^H \\ &= \sum_{k=1}^{K} \gamma_k \boldsymbol{b}(\beta_k)\boldsymbol{a}^T(\alpha_k) + \bar{\boldsymbol{W}} \\ &= \boldsymbol{B}(\beta)\boldsymbol{\Lambda}(\gamma)\boldsymbol{A}^T(\alpha) + \bar{\boldsymbol{W}}\end{aligned} \tag{2}$$

where $\boldsymbol{\Lambda}(\gamma) = diag[\gamma_1, \gamma_2, \cdots, \gamma_K]$ denotes the reflection coefficients matrix, $\boldsymbol{B}(\beta) = [\boldsymbol{b}(\beta_1), \boldsymbol{b}(\beta_2), \cdots, \boldsymbol{b}(\beta_K)]$ and $\boldsymbol{A}(\alpha) = [\boldsymbol{a}(\alpha_1), \boldsymbol{a}(\alpha_2), \cdots, \boldsymbol{a}(\alpha_K)]$ denote the receive and transmit steering matrix, respectively. Let $\boldsymbol{S}(\gamma) = \boldsymbol{\Lambda}(\gamma)\boldsymbol{A}^T(\alpha) \in \mathbb{C}^{K\times M}$, the received model in (2) can be further expressed as

$$\bar{\boldsymbol{X}} = \boldsymbol{B}(\beta)\boldsymbol{S}(\gamma) + \bar{\boldsymbol{W}} \tag{3}$$

From (3), we can find that the model behaves like a multiple snapshots ULA received model. But, the received data in (3) is only a single snapshot data for bistatic MIMO radars. Assuming that the total number of snapshots is L, in oder to use the advantages of the angular decouple in (3), by collecting all snapshopts together, the received data becomes

$$\hat{\boldsymbol{X}} = \boldsymbol{B}(\beta)\hat{\boldsymbol{S}}(\gamma) + \hat{\boldsymbol{W}} \tag{4}$$

where

$$\hat{\boldsymbol{S}}(\gamma) = \begin{bmatrix} \gamma_1(1)\boldsymbol{a}^T(\alpha_1) & \cdots & \gamma_1(L)\boldsymbol{a}^T(\alpha_1) \\ \gamma_2(1)\boldsymbol{a}^T(\alpha_2) & \cdots & \gamma_2(L)\boldsymbol{a}^T(\alpha_2) \\ \vdots & \ddots & \vdots \\ \gamma_K(1)\boldsymbol{a}^T(\alpha_K) & \cdots & \gamma_K(L)\boldsymbol{a}^T(\alpha_K) \end{bmatrix} \in \mathbb{C}^{K\times ML} \tag{5}$$

It can be found that the new model in (4) can separate the DOA and DOD. Thus, the high resolution sparse recovery methods used in the one-dimensional angular parameter estimation for ULA can be directly applied to DOA estimation in the bistatic MIMO radar. The detailed sparse recovery algorithm will be introduced in the next Section. Now, we will construct another new signal model for DOD to realize the accuracy angular estimation.

By using the vectorization operation on (2), we can obtain an $MN \times 1$ virtual data vector as follows

$$\boldsymbol{Y} = vec(\bar{\boldsymbol{X}}) = [\boldsymbol{A}(\alpha) \odot \boldsymbol{B}(\beta)]\boldsymbol{\gamma} + \boldsymbol{w} \tag{6}$$

where $\boldsymbol{\gamma} = [\gamma_1, \gamma_2, \cdots, \gamma_K]^T \in \mathbb{C}^{K\times 1}$, $\boldsymbol{w} = vec\left(\bar{\boldsymbol{W}}\right)$. And there exists a permutation matrix $\boldsymbol{\Pi} \in \mathbb{R}^{MN\times MN}$, satisfying

$$\boldsymbol{\Pi}[\boldsymbol{A}(\alpha) \odot \boldsymbol{B}(\beta)] = \boldsymbol{B}(\beta) \odot \boldsymbol{A}(\alpha) \tag{7}$$

and

$$\bar{\boldsymbol{Y}} = \boldsymbol{\Pi}\boldsymbol{Y} = (\boldsymbol{B}(\beta) \odot \boldsymbol{A}(\alpha))\,\boldsymbol{\gamma} + \bar{\boldsymbol{w}} \tag{8}$$

For matrices of $\boldsymbol{Y}_1 \in \mathbb{C}^{M1\times M2}$,$\boldsymbol{Y}_2 \in \mathbb{C}^{M2\times M3}$ and $\boldsymbol{Y}_3 \in \mathbb{C}^{M3\times M4}$, the equation $vec\{\boldsymbol{Y}_1\boldsymbol{Y}_2\boldsymbol{Y}_3\} = (\boldsymbol{Y}_3^T \otimes \boldsymbol{Y}_1)\,vec\,(\boldsymbol{Y}_2)$ can be obtained by using the relationship between the Kronecker product and vectorization operation. Due to this special characteristic, (8) can be further expressed as (9) at the top of the next page.

Define a matrix $\hat{\boldsymbol{Y}} \in \mathbb{C}^{M\times N}$ and the matrix $\hat{\boldsymbol{Y}}$ satisfies $\bar{\boldsymbol{Y}} = vec(\hat{\boldsymbol{Y}})$. Thus, from (9), we can find that

$$\begin{aligned} vec(\hat{\boldsymbol{Y}}) &= (\boldsymbol{B}(\beta) \otimes \boldsymbol{I}_N)vec(\tilde{\boldsymbol{S}}(\gamma)) + \bar{\boldsymbol{w}} \\ &= vec\left(\boldsymbol{I}_N\tilde{\boldsymbol{S}}(\gamma)\boldsymbol{B}^T(\beta) + \tilde{\boldsymbol{W}}_1\right) \end{aligned} \tag{10}$$

where $\tilde{\boldsymbol{S}}(\gamma) = [\boldsymbol{a}(\alpha_1)\gamma_1, \boldsymbol{a}(\alpha_2)\gamma_2, \cdots, \boldsymbol{a}(\alpha_K)\gamma_K] \in \mathbb{C}^{M\times K}$, $\tilde{\boldsymbol{W}}_1$ satisfies $\bar{\boldsymbol{w}} = vec(\tilde{\boldsymbol{W}}_1)$. Thus,

$$\begin{aligned} \hat{\boldsymbol{Y}} &= \tilde{\boldsymbol{S}}(\gamma)\boldsymbol{B}^T(\beta) + \tilde{\boldsymbol{W}}_1 \\ &= [\boldsymbol{a}(\alpha_1)\gamma_1, \boldsymbol{a}(\alpha_2)\gamma_2, \cdots, \boldsymbol{a}(\alpha_K)\gamma_K] \begin{bmatrix} \boldsymbol{b}^T(\beta_1) \\ \boldsymbol{b}^T(\beta_2) \\ \vdots \\ \boldsymbol{b}^T(\beta_K) \end{bmatrix} + \tilde{\boldsymbol{W}}_1 \\ &= [\boldsymbol{a}(\alpha_1), \boldsymbol{a}(\alpha_2), \cdots, \boldsymbol{a}(\alpha_K)] \begin{bmatrix} \gamma_1\boldsymbol{b}^T(\beta_1) \\ \gamma_2\boldsymbol{b}^T(\beta_2) \\ \vdots \\ \gamma_K\boldsymbol{b}^T(\beta_K) \end{bmatrix} + \tilde{\boldsymbol{W}}_1 \\ &= \boldsymbol{A}(\alpha)\hat{\boldsymbol{S}}_1(\gamma) + \tilde{\boldsymbol{W}}_1 \end{aligned} \tag{11}$$

where $\hat{\boldsymbol{S}}_1(\gamma) = \left[\gamma_1\boldsymbol{b}^T(\beta_1), \gamma_2\boldsymbol{b}^T(\beta_2), \cdots, \gamma_K\boldsymbol{b}^T(\beta_K)\right]^T \in \mathbb{C}^{K\times N}$, $\tilde{\boldsymbol{W}}_1 \in \mathbb{C}^{M\times N}$. It can be founded that the signal model in (11) has the same structure as (3) under the condition of single snapshot. Thus, we can also stack all snapshots together to form a more large measurement matrix for DOD as follows

$$\hat{\boldsymbol{Y}}_1 = \boldsymbol{A}(\alpha)\hat{\boldsymbol{S}}_2(\gamma) + \tilde{\boldsymbol{W}}_2 \tag{12}$$

where

$$\hat{\boldsymbol{S}}_2(\gamma) = \begin{bmatrix} \gamma_1(1)\boldsymbol{b}^T(\beta_1) & \cdots & \gamma_1(L)\boldsymbol{b}^T(\beta_1) \\ \gamma_2(1)\boldsymbol{b}^T(\beta_2) & \cdots & \gamma_2(L)\boldsymbol{b}^T(\beta_2) \\ \vdots & \ddots & \vdots \\ \gamma_K(1)\boldsymbol{b}^T(\beta_K) & \cdots & \gamma_K(L)\boldsymbol{b}^T(\beta_K) \end{bmatrix} \in \mathbb{C}^{K\times NL} \tag{13}$$

$$\begin{aligned}\bar{\boldsymbol{Y}} &= (\boldsymbol{B}(\beta) \odot \boldsymbol{A}(\alpha))\,\boldsymbol{\gamma} + \bar{\boldsymbol{w}} \\ &= [\boldsymbol{b}(\beta_1) \otimes \boldsymbol{a}(\alpha_1), \boldsymbol{b}(\beta_2) \otimes \boldsymbol{a}(\alpha_2), \cdots, \boldsymbol{b}(\beta_K) \otimes \boldsymbol{a}(\alpha_K)]\,\boldsymbol{\gamma} + \bar{\boldsymbol{w}} \\ &= \left[vec\left(\boldsymbol{a}(\alpha_1)\boldsymbol{b}^T(\beta_1)\right), vec\left(\boldsymbol{a}(\alpha_2)\boldsymbol{b}^T(\beta_2)\right), \cdots, vec\left(\boldsymbol{a}(\alpha_K)\boldsymbol{b}^T(\beta_K)\right)\right]\boldsymbol{\gamma} + \bar{\boldsymbol{w}} \\ &= [(\boldsymbol{b}(\beta_1) \otimes \boldsymbol{I}_N)\,\boldsymbol{a}(\alpha_1), (\boldsymbol{b}(\beta_2) \otimes \boldsymbol{I}_N)\,\boldsymbol{a}(\alpha_2), \cdots, (\boldsymbol{b}(\beta_K) \otimes \boldsymbol{I}_N)\,\boldsymbol{a}(\alpha_K)]\,\boldsymbol{\gamma} + \bar{\boldsymbol{w}} \\ &= [\boldsymbol{b}(\beta_1), \boldsymbol{b}(\beta_2), \cdots, \boldsymbol{b}(\beta_K)] \otimes \boldsymbol{I}_N \left[\boldsymbol{a}^T(\alpha_1)\gamma_1, \boldsymbol{a}^T(\alpha_2)\gamma_2, \cdots, \boldsymbol{a}^T(\alpha_K)\gamma_K\right] + \bar{\boldsymbol{w}} \end{aligned} \tag{9}$$

It is obvious that (4) and (12) have the similar form and the constructed two new received models can avoid the coupled problem for DOD and DOA. Thus, the sparse recovery algorithm can be applied to (4) and (12) without discreting the whole two-dimensional angular area. Here we can find that $\hat{\boldsymbol{X}}$ and $\hat{\boldsymbol{Y}}_1$ can be solved in a similar manner. Thus, in the following analysis, we only derive the sparse recovery solution for (12). The solution for (4) can be obtained in the same way and the corresponding process is omitted in this paper.

III. SPARSITY BASED METHOD FOR BISTATIC MIMO RADAR

A. SPARSITY BASED ESTIMATOR

According to (12),we can use the sparse recovery method to resolve the DOD in bistatic MIMO radar due to the angular position is sparsely distributed over the whole angular area. Thus, an over-complete dictionary can be constructed by discreting the potential angular area from $-90°$ to $-90°$. Furthermore, we assume that the true DODs are exactly aligned with the sampling angular grid. Thus, $\hat{\boldsymbol{Y}}_1$ in (12) can be rewritten as

$$\hat{\boldsymbol{Y}}_1 = \hat{\boldsymbol{A}}(\alpha)\tilde{\boldsymbol{S}} + \boldsymbol{N} \tag{14}$$

where $\hat{\boldsymbol{A}}(\alpha) = [\hat{\boldsymbol{a}}(\alpha)_1, \hat{\boldsymbol{a}}(\alpha)_2, \cdots, \hat{\boldsymbol{a}}(\alpha)_Q] \in \mathbb{C}^{M\times Q}$, Q denotes the number of the sampling grid, and $\tilde{\boldsymbol{S}} = [\tilde{\boldsymbol{s}}(\alpha)_1, \tilde{\boldsymbol{s}}(\alpha)_2, \cdots, \tilde{\boldsymbol{s}}(\alpha)_Q]^T \in \mathbb{C}^{Q\times NL}$ with $\tilde{\boldsymbol{s}}(\alpha)_q = [\tilde{s}(1), \tilde{s}(2), \cdots, \tilde{s}(NL)]^T \in \mathbb{C}^{\tilde{NL}}$. The data model in (14) is referred to as multiple measurement vectors (MMVs). In the case of multiple snapshots, the rows of $\tilde{\boldsymbol{S}}$ satisfy the joint sparsity. Thus, the true DODs can be estimated by using those grid points of α corresponding to the nonzero rows of $\tilde{\boldsymbol{S}}$. The temporal redundancy of MMV model can further improve the estimation performance for the sparse representation techniques. Since the MMV data model in (14) is quite general, the joint sparse signal recovery probelm can be directly solved by the $\ell_{2,0}$-norm sparse optimization algorithm. But, the $\ell_{2,0}$ sparse optimization problem is non-convex and NP-hard. Alternatively, the tightest convex relaxation $\ell_{2,1}$ optimization method is proposed to resolve the joint sparse signal recovery probelm in [30]. Unfortunately, the relaxation error cannot be ignored when the ℓ_2-norms of the the nonzero rows in $\tilde{\boldsymbol{S}}$ exhibit different values. In order to circumvent these disadvantages existed in the $\ell_{2,0}$-norm and $\ell_{2,1}$-norm sparse optimization algorithms, a covariance sparsity-aware estimator is proposed to realize the angular parameter estimation for DOD. And, we can also eliminate the effect of the noise by using the structure of the noise covariance matrix. So, better estimation accuracy of the proposed method can be guaranteed.

In practice, the sample covariance matrix is estimated by finite snapshots, which can be expressed as

$$\hat{\boldsymbol{R}} = \frac{1}{NL}\sum_{t=1}^{NL}\hat{\boldsymbol{Y}}_1\hat{\boldsymbol{Y}}_1^H = \hat{\boldsymbol{A}}(\alpha)\boldsymbol{R}_s\hat{\boldsymbol{A}}^H(\alpha) + \boldsymbol{R}_n + \boldsymbol{E} \tag{15}$$

where $\boldsymbol{R}_s = \mathbb{E}[\tilde{\boldsymbol{S}}\tilde{\boldsymbol{S}}^H]$ denotes the signal covariance matrix, $\boldsymbol{R}_n = \mathbb{E}[\tilde{\boldsymbol{W}}_2\tilde{\boldsymbol{W}}_2^H]$ denotes the noise covariance matrix and $\boldsymbol{E}$ denots the perturbation errors between the estimated covariance matrix and the theoretical covariance matrix due to the finite number of snapshots. By adopting vectorization operation to (15), a virtual long vector can be obtained as

$$\boldsymbol{r} = vec(\hat{\boldsymbol{R}}) = \boldsymbol{\Psi}\boldsymbol{\rho} + \boldsymbol{\epsilon} + \boldsymbol{\xi} \tag{16}$$

where $\boldsymbol{\Psi} = \hat{\boldsymbol{A}}^*(\alpha) \odot \hat{\boldsymbol{A}}(\alpha)$, $\boldsymbol{\rho} = vec(\boldsymbol{R}_s)$,$\boldsymbol{\epsilon} = vec(\boldsymbol{E})$ and $\boldsymbol{\xi} = vec(\boldsymbol{R}_n)$. Compared (16) with (14), it can be obviously found that the MMV data model is converted to single measurement vector (SMV) data model. Thus, the DOD estimation problem turns out to be that of recovering the sparse vector $\boldsymbol{\rho}$ and detecting the locations of nonzero elements of this vector.

Due to the noises satisfy zero-mean, complex circular Gaussian characteristic and the noises are statistically independent of all targets in bistatic MIMO radar, thus the sturcture of the noise covariance matrix is a diagonal matrix. This means that the positions of the nonzero element in $\boldsymbol{\xi}$ can be determined. Therefore, in order to further improve the estimated performance, the effect of the noises can be eliminated by using a selecting matrix $\boldsymbol{J} \in \mathbb{C}^{M(M-1)\times M^2}$ as follows

$$\boldsymbol{u} = \boldsymbol{J}\boldsymbol{r} = \boldsymbol{J}\boldsymbol{\Psi}\boldsymbol{\rho} + \boldsymbol{J}\boldsymbol{\epsilon} \tag{17}$$

where

$$\boldsymbol{J} = [\boldsymbol{J}_1, \boldsymbol{J}_2, \cdots, \boldsymbol{J}_{M-1}]^T \tag{18}$$

and

$$\boldsymbol{J}_m = \left[\boldsymbol{e}_{(m-1)(M+1)+2}, \boldsymbol{e}_{(m-1)(M+1)+3}, \cdots, \boldsymbol{e}_{m(M+1)}\right] \tag{19}$$

for $m = 1, 2, \cdots, M$. And, $\boldsymbol{e}_i(i = (m-1)(M+1)+2, (m-1)(M+1)+3, \cdots, m(M+1))$ is an $M^2 \times 1$ column vector with 1 at the i-th position and 0 elsewhere.

For the perturbation errors vector $\boldsymbol{\epsilon}$, as derived in [31], [32], its asymptotically norm distribution (AsN) satisfies

$\boldsymbol{\epsilon} \sim \mathcal{CN}(\mathbf{0}, \hat{\boldsymbol{R}}^T \otimes \hat{\boldsymbol{R}}/NL)$. Thus, the distribution of $\boldsymbol{J\epsilon}$ satisfies $\mathcal{CN}(\mathbf{0}, \boldsymbol{G})$ with $\boldsymbol{G} = (\boldsymbol{J}(\hat{\boldsymbol{R}}^T \otimes \hat{\boldsymbol{R}})\boldsymbol{J}^H)/NL$. Obviously, a whitening filter $\boldsymbol{G}^{-\frac{1}{2}}$ can be adopted to alleviate the effect of the perturbation errors vector, namely

$$\hat{\boldsymbol{u}} = \boldsymbol{G}^{-\frac{1}{2}}\boldsymbol{u} = \boldsymbol{\Phi\rho} + \boldsymbol{v} \tag{20}$$

where $\boldsymbol{\Phi} = \boldsymbol{G}^{-\frac{1}{2}}\boldsymbol{J\Psi}$ and the new perturbation errors vector $\boldsymbol{v} = \boldsymbol{G}^{-\frac{1}{2}}\boldsymbol{J\epsilon} \sim \mathcal{CN}(\mathbf{0}, \boldsymbol{I}_{M(M-1)})$. Thus, after the noise suppresion and whitening filter operation, the optimization problem for finding the nonzero elements in $\boldsymbol{\rho}$ can be described as

$$\min_{\boldsymbol{\rho}} \left\{ \frac{1}{2} \left\| \hat{\boldsymbol{u}} - \boldsymbol{\Phi\rho} \right\|_2^2 + \tau \left\| \boldsymbol{\rho} \right\|_1 \right\}, \quad s.t. \quad \boldsymbol{\rho} \succeq \mathbf{0} \tag{21}$$

where $\tau \geq 0$ denotes the regularization parameter and the appropriate choice of τ can improve the angular estimation performance. In (21), the convex relaxation ℓ_1-norm optimization method is proposed to resolve the sparse signal recovery probelm. However, for the vectorization model (16), the nonzero elements values in $\boldsymbol{\rho}$ which denotes the target powers may be different. In oder to achieve better estimation performance, we design a reweighted alternative optimization algorithm as follows

$$\min_{\boldsymbol{\rho}} \left\{ \frac{1}{2} \left\| \hat{\boldsymbol{u}} - \boldsymbol{\Phi\rho} \right\|_2^2 + \tau \sum_{i=0}^{Q-1} \omega_i |\rho_i| \right\}, \quad s.t. \quad \boldsymbol{\rho} \succeq \mathbf{0} \tag{22}$$

where ρ_i denotes the i-th element of ρ and ω_i is the weight coefficient to guarantee the better sparsity solution. According to the analysis in [33], ρ_i satisfies $\rho_i \leq NL/(\hat{\boldsymbol{a}}(\alpha)_i^H \hat{\boldsymbol{R}}^{-1} \hat{\boldsymbol{a}}(\alpha)_i)$. Thus, we choose the weight coefficient ω_i as $\omega_i = (\hat{\boldsymbol{a}}(\alpha)_i^H \hat{\boldsymbol{R}}^{-1} \hat{\boldsymbol{a}}(\alpha)_i)/NL$. The machanism of the weight coefficient lies that the large weight coefficients can punish the elements who are more likely to be zeros in the sparse vector $\boldsymbol{\rho}$, in contrast, small weights reserve the larger entries. In other words, the weight coefficient operation can improve the angular estimation accuracy by punishing the sparsity of the elements in $\boldsymbol{\rho}$. But, the better estimation performance also relies on the selection of the regularization parameter τ. In order to avoid the disadvantages of the heuristic methods in [34], an appropriate selection of τ is required to guarantee the robust sparse recovery, which will be investigated in the next subsection.

B. REGULARIZATION PARAMETER SELECTION

The selection of the regularization parameter is very important for the final sparse receovery performance because it can balance the sparsity and the data fidelity. For example, an poor choice may lead to wrong angular parameter estimation or generate many false peaks. In order to set a suitable regularization parameter value, we will derive the regularization parameter with the help of the Largrangian duality.

Firstly, the sparse recovery problem in (22) can be rewritten as

$$\begin{aligned} &\min_{\boldsymbol{\rho}} \left\{ \frac{1}{2} \left\| \boldsymbol{\zeta} \right\|_2^2 + \tau \sum_{i=0}^{Q-1} \omega_i |\rho_i| \right\} \\ &s.t. \quad \boldsymbol{\zeta} = \hat{\boldsymbol{u}} - \boldsymbol{\Phi\rho}, \quad \boldsymbol{\rho} \succeq \mathbf{0} \end{aligned} \tag{23}$$

Then, by introducing $\boldsymbol{\mu}$ and $\boldsymbol{\lambda}$ as the Lagrangian multipliers and formulating the augmented Lagrange function for (23) as

$$\min_{\boldsymbol{\rho}} \left\{ \frac{1}{2} \left\| \boldsymbol{\zeta} \right\|_2^2 + \tau \sum_{i=0}^{Q-1} \omega_i |\rho_i| + \boldsymbol{\mu}^T(\boldsymbol{\zeta} - \hat{\boldsymbol{u}} + \boldsymbol{\Phi\rho}) - \boldsymbol{\lambda}^T\boldsymbol{\rho} \right\} \tag{24}$$

where $\boldsymbol{\mu}$ is the Lagrange multiplier corresponding to the equality constraint $\boldsymbol{\zeta} = \hat{\boldsymbol{u}} - \boldsymbol{\Phi\rho}$, $\boldsymbol{\lambda} \succeq \mathbf{0}$ is the Lagrange multiplier corresponding to the inequality constraint $\boldsymbol{\rho} \succeq \mathbf{0}$. For fixed $\boldsymbol{\rho}$, the minimization of the augmented Lagrange function w.r.t the vector $\boldsymbol{\zeta}$ can be expressed as

$$\boldsymbol{\mu} = -\boldsymbol{\zeta} = -(\hat{\boldsymbol{u}} - \boldsymbol{\Phi\rho}) \tag{25}$$

Thus, the vector $\boldsymbol{\zeta}$ can be eliminated by substituting (25) into (24). Sequentially, the new augmented Lagrange function can be denoted as

$$\min_{\boldsymbol{\rho}} \left\{ \frac{1}{2} \left\| \boldsymbol{\mu} \right\|_2^2 + \tau \sum_{i=0}^{Q-1} \omega_i |\rho_i| + \boldsymbol{\mu}^T\boldsymbol{\Phi\rho} - \boldsymbol{\mu}^T\hat{\boldsymbol{u}} - \boldsymbol{\lambda}^T\boldsymbol{\rho} \right\} \tag{26}$$

Furthermore, in order to obtain the regularization parameter τ , the duality of the augmented Lagrange function is adopted. The minimization of (26) is equivalent to the maximization its duality function

$$\begin{aligned} &\max_{\boldsymbol{\mu},\boldsymbol{\lambda}} \left\{ \frac{1}{2} \left\| \boldsymbol{\mu} \right\|_2^2 - \boldsymbol{\mu}^T\hat{\boldsymbol{u}} + \inf_{\boldsymbol{\rho}}[\mathcal{L}(\boldsymbol{\rho}, \boldsymbol{\mu}, \boldsymbol{\lambda})] \right\} \\ &s.t. \quad \mathcal{L}(\boldsymbol{\rho}, \boldsymbol{\mu}, \boldsymbol{\lambda}) = \tau \sum_{i=0}^{Q-1} \omega_i |\rho_i| + \boldsymbol{\mu}^T\boldsymbol{\Phi\rho} - \boldsymbol{\lambda}^T\boldsymbol{\rho} \end{aligned} \tag{27}$$

where inf denotes the infimum and $\inf_{\boldsymbol{\rho}}[\mathcal{L}(\boldsymbol{\rho}, \boldsymbol{\mu}, \boldsymbol{\lambda})]$ means that minimum over $\boldsymbol{\rho}$ for fixed $\boldsymbol{\mu}$ and $\boldsymbol{\lambda}$. The $Karush-Kuhn-Tucker(KKT)$ condition is the essential condition for the strong dual optimization. Thus, by using the KKT condition, the last term of the $\inf_{\boldsymbol{\rho}}[\mathcal{L}(\boldsymbol{\rho}, \boldsymbol{\mu}, \boldsymbol{\lambda})]$ satisfies $\boldsymbol{\lambda}^T\boldsymbol{\rho} = 0$ [35]. Then, the infimum of $\mathcal{L}(\boldsymbol{\rho}, \boldsymbol{\mu}, \boldsymbol{\lambda})$ can be redenoted as

$$\begin{aligned} &\sum_{i=0}^{Q-1} \inf_{\rho_i}[\delta_i] \\ &s.t. \quad \delta_i = \tau\mu_i|\rho_i| + \eta_i\rho_i \end{aligned} \tag{28}$$

where $\eta_i = \boldsymbol{\phi_i}^T\boldsymbol{\mu} = -\boldsymbol{\phi_i}^T(\hat{\boldsymbol{u}} - \boldsymbol{\Phi\rho})$ denotes the i-th element of $\boldsymbol{\mu}^T\boldsymbol{\Phi}$ and $\boldsymbol{\phi_i}$ denotes the i-th column of $\boldsymbol{\Phi}$. In order to determine the minimum of the δ_i, the absolute value of ρ_i should be removed. Then,

$$\delta_i = \begin{cases} \tau\mu_i\rho_i + \eta_i\rho_i, & if \ \rho_i \geq 0 \\ -\tau\mu_i\rho_i + \eta_i\rho_i, & if \ \rho_i < 0 \end{cases} \tag{29}$$

From (29), it can be found that the mathematical essence of the above equation is to find the minimum value of the one-dimensional linear function. Thus, the infimum of δ_i can be expressed as

$$\inf_{\rho_i}[\delta_i] = \begin{cases} 0, & if \quad \tau\mu_i \geq |\eta_i| \\ -\infty, & otherwise \end{cases} \tag{30}$$

Since $\inf_{\rho_i}[\delta_i] = -\infty$ is meaningless for the sparse optimization problem. Hence, infimum of δ_i is 0. The constraint on regularization parameter τ can be denoted as

$$\tau\mu_i \geq |\eta_i| = \sqrt{\left\{\boldsymbol{\phi_i}^T(\hat{\boldsymbol{u}} - \boldsymbol{\Phi\rho})(\boldsymbol{\phi_i}^T(\hat{\boldsymbol{u}} - \boldsymbol{\Phi\rho}))^H\right\}} \quad i = 0, 1, \cdots, Q-1 \tag{31}$$

As discussed in (20), the perturbation error vector $\boldsymbol{v}$ satisfies $\boldsymbol{v} = \boldsymbol{G}^{-\frac{1}{2}}\boldsymbol{J\epsilon} \sim \mathcal{CN}(\boldsymbol{0}, \boldsymbol{I}_{M(M-1)})$, namely, $\hat{\boldsymbol{u}} - \boldsymbol{\Phi\rho} \sim \mathcal{CN}(\boldsymbol{0}, \boldsymbol{I}_{M(M-1)})$. Thus, the distribution $\boldsymbol{\phi_i}^T(\hat{\boldsymbol{u}} - \boldsymbol{\Phi\rho})$ is $\mathcal{CN}(\boldsymbol{0}, \boldsymbol{\phi_i}^T\boldsymbol{\phi_i})$. A prewhitening operation on $\boldsymbol{\phi_i}^T(\hat{\boldsymbol{u}} - \boldsymbol{\Phi\rho})$ yields

$$\sqrt{\left\{2/(\boldsymbol{\phi_i}^T\boldsymbol{\phi_i})\right\}}\boldsymbol{\phi_i}^T(\hat{\boldsymbol{u}} - \boldsymbol{\Phi\rho}) \sim \mathcal{CN}(\boldsymbol{0}, 2) \tag{32}$$

By using the relationship betweenn the chi-square distribution and the standard normal distribution, the distribution of $\boldsymbol{\phi_i}^T(\hat{\boldsymbol{u}} - \boldsymbol{\Phi\rho})(\boldsymbol{\phi_i}^T(\hat{\boldsymbol{u}} - \boldsymbol{\Phi\rho}))^H$ can be denoted as

$$\left\{2/(\boldsymbol{\phi_i}^T\boldsymbol{\phi_i})\right\}\boldsymbol{\phi_i}^T(\hat{\boldsymbol{u}} - \boldsymbol{\Phi\rho})(\boldsymbol{\phi_i}^T(\hat{\boldsymbol{u}} - \boldsymbol{\Phi\rho}))^H \sim \chi^2(2) \tag{33}$$

where $\chi^2(2)$ denotes the chi-square distribution with 2 DOF.

In order to use the obtained chi-square distribution, a suitable threshold value κ is chosen to make its probability almost equal to one. Namely,

$$Pr(\chi^2(2) \leq \kappa) = P_\kappa \approx 1 \tag{34}$$

Then, substituting (31) and (33) into (34) yields

$$Pr(2/(\boldsymbol{\phi_i}^T\boldsymbol{\phi_i})|\eta_i|^2 \leq \kappa) = Pr(|\eta_i| \leq \frac{\sqrt{\boldsymbol{\phi_i}^T\boldsymbol{\phi_i}}}{\sqrt{2}}\sqrt{\kappa}) = P_\kappa \tag{35}$$

Therefore, the regularisation parameter τ can be chosen as

$$\tau \geq \frac{\sqrt{\boldsymbol{\phi_i}^T\boldsymbol{\phi_i}}}{\sqrt{2}\mu_i}\sqrt{\kappa} \tag{36}$$

And the relationship in (31) can be satisfied with a probability close to one. Thus, for all the Q inequality constraints in (31), the final regularization parameter τ is adopted as

$$\tau = \max_i \left(\frac{\sqrt{\boldsymbol{\phi_i}^T\boldsymbol{\phi_i}}}{\sqrt{2}\mu_i}\right)\sqrt{\kappa} \tag{37}$$

Finally, the original sparse recovery algorithm in (22) can be efficiently solved with the appropriate regularization parameter selected in (37) by off-the-shelf optimization softwares, e.g., the CVX [36]. In order to make the proposed method comprehensible, the procedure of our algorithm is summarized in Algorithm 1.

Algorithm 1 summary of the Proposed Method

Require: array received data $\hat{\boldsymbol{X}} \in \mathbb{C}^{N\times ML}$, threshold value $\kappa \in (0, 1)$

Ensure: estimated DODs $\hat{\alpha}$ and estimated DOAs $\hat{\beta}$

1: Construct the new signal model $\hat{\boldsymbol{Y}}_1$ for DOD by using the relationship between the Kronecker product and vectorization operation according to (6)-(12).
2: Calculate the covariance matrix $\hat{\boldsymbol{R}}$ and virtual long vector $\boldsymbol{r}$ according to (15) and (16), respectively.
3: Construct the selecting matrix $\boldsymbol{J} \in \mathbb{C}^{M(M-1)\times M^2}$ according to (18) and the whitening filter $\boldsymbol{G} = (\boldsymbol{J}(\hat{\boldsymbol{R}}^T \otimes \hat{\boldsymbol{R}})\boldsymbol{J}^H)/NL$.
4: Calculate the new vector $\hat{\boldsymbol{u}}$ by using the constructed selecting matrix $\boldsymbol{J}$ and the whitening filter $\boldsymbol{G}$ according to (20).
5: After obtaining the new vector $\hat{\boldsymbol{u}}$, construct the sparse optimization problem according to (21) and the reweighted alternative algorithm according to (22).
6: Calculate the regularization parameter τ with the aid of the Largrangian duality theory and the final regularization parameter is adopted as $\tau = \max_i\left(\frac{\sqrt{\boldsymbol{\phi_i}^T\boldsymbol{\phi_i}}}{\sqrt{2}\mu_i}\right)\sqrt{\kappa}$.
7: Calculate the estimated DODs $\hat{\alpha}$ by solving the reweighted alternative algorithm according to (22), the corresponding signal directions are indexed by the nonzero values in $\boldsymbol{\rho}$.
8: The estimated DOAs $\hat{\beta}$ can be obtained in the same way by repeating Step.2 to Step.7 if the DODs and DOAs of the imping targets are in ascending order or descending order.
9: If the DODs and DOAs of the imping targets are out of order, construct the orthogonality relation between the signal subspace and the noise subspace accoring to (44).
10: Construct the constrained relationship between α and β according to (45) and (46) by using the Kronecker product and vectorization operation.
11: Get the estimated receive steering vector $\hat{\boldsymbol{b}}(\beta)$ according to (49) by using the estimated DODs $\hat{\alpha}$ obtained in Step.7.
12: Calculate the estimated DOAs $\hat{\beta}$ according to (50) and (51) by using the shift invariance relationship.

C. RELATED REMARKS

Remark 1: The computational complexity of the proposed method mainly contains the calculation of the covariance matrix, selecting matrix operation, the whitening filter operation, over-complete dictionary construction and reweighted alternative convex optimization process by using the CVX, which are required an amount of complex multiplications of $\mathcal{O}(M^2NL + N^2ML)$, $\mathcal{O}(M^3 + N^3)$, $\mathcal{O}(M^5 + N^5)$,$\mathcal{O}(KM^6 + KN^6)$ and $\mathcal{O}(Q^3M(M-1) + Q^3N(N-1)$, respectively. Thus, the total computational complexity of the proposed method is $\mathcal{O}(M^2NL + N^2ML + M^3 + N^3 + M^5 + N^5 + KM^6 + KN^6 + Q^3M(M-1) + Q^3N(N-1)$. Besides the proposed method, the computational

TABLE 1. Comparison of the complexity.

Method	Complexity	Average Run time(s)
RD-MUSIC	$\mathcal{O}(LM^2N^2 + M^3N^3 + Q$ $[(M^2N + M^2)(MN - K)$ $+M^2])$	0.0251
RD-Capon	$\mathcal{O}(LM^2N^2 + M^3N^3 + Q$ $[M^3N^2 + M^2N^3 + M^3N$ $+N^3M + M^2 + N^2])$	0.0492
ESPRIT	$\mathcal{O}(LM^2N^2 + M^3N^3 + 2$ $K^2(N-1)M + 2K^2(M-$ $1) + 6K^3)$	0.0058
Proposed	$\mathcal{O}(M^2NL + N^2ML + M^3$ $+N^3 + M^5 + N^5 + KM^6$ $+KN^6 + Q^3M(M-1)+$ $Q^3N(N-1)$	1.7421

complexity of the RD-MUSIC algorithm, RD-Capon algorithm and ESPRIT algorithm are also discussed for comparisons. The computational complexity of the RD-MUSIC algorithm mainly contains the covariance matrix, the eigenvalue decomposition and one dimensional peak search process, which are required an amount of complex multiplications of $\mathcal{O}(LM^2N^2)$, $\mathcal{O}(M^3N^3)$ and $\mathcal{O}(Q[(M^2N + M^2)(MN - K) + M^2])$, respectively. Thus, the total computational complexity of the RD-MUSIC algorithm is $\mathcal{O}(LM^2N^2 + M^3N^3 + Q[(M^2N + M^2)(MN - K) + M^2])$. The computational complexity of the RD-Capon algorithm mainly contains the covariance matrix, matrix inversion operation and two one dimensional peak search process, which are required an amount of complex multiplications of $\mathcal{O}(LM^2N^2)$, $\mathcal{O}(M^3N^3)$ and $\mathcal{O}(Q[M^3N^2 + M^2N^3 + M^3N + N^3M + M^2 + N^2])$, respectively. Thus, the total computational complexity of the RD-Capon algorithm is $\mathcal{O}(LM^2N^2 + M^3N^3 + Q[M^3N^2 + M^2N^3 + M^3N + N^3M + M^2 + N^2])$. The computational complexity of the ESPRIT algorithm mainly contains the covariance matrix, the eigenvalue decomposition and the construction of the rotational invariance relationship for DOD and DOA, which are required an amount of complex multiplications of $\mathcal{O}(LM^2N^2)$, $\mathcal{O}(M^3N^3)$ and $\mathcal{O}(2K^2(N-1)M + 2K^2(M-1) + 6K^3)$, respectively. Thus, the total computational complexity of the ESPRIT algorithm is $\mathcal{O}(LM^2N^2 + M^3N^3 + 2K^2(N-1)M + 2K^2\,(M-1) + 6K^3)$. In order to provide an intuitive complexity comparison, the average MATLAB running time of four methods are also provided. The processing time is calculated by the MATLAB R2016a under the conditional of Intel Core i7-7700 central processing unit @3.6 GHz and 3.6GB random access memory and 8GB RAM. The simulation parameters for RD-MUSIC algorithm, RD-Capon algorithm and ESPRIT algorithm are the same as the first experiment in Section IV. As shown in Table 1, the proposed algorithm has the highest computational efficiency due to the convex optimization process. Meanwhile, the ESPRIT algorithm is the most computationally efficient as it obtains estimates with closed-form solutions.

Remark 2: The maximal number of identified targets is an important aspect that should be considered for the developed sparse recovery-based method. We note that the dimension of the virtual manifold matrix $\boldsymbol{\Phi}$ is $M(M-1)$, which may improve the degrees of freedom (DOF) of the original linear array. This motivates us to discuss the problem of maximum number of resolvable targets of the proposed method based on (20). As shown in (20), the angular estimation problem relies on the sparsity of the vector $\boldsymbol{\rho}$. According to the difference co-array principle [37], the maximum DOF achievable in $\boldsymbol{\Psi} = \hat{\boldsymbol{A}}^*(\alpha) \odot \hat{\boldsymbol{A}}(\alpha)$ satisfies $DOF_{max} = 2(M-1)+1$ for M-element ULA. Note that the matrix $\hat{\boldsymbol{A}}^*(\alpha) \odot \hat{\boldsymbol{A}}(\alpha)$ contain many repeating row vectors, thus, pre-multiplying $\boldsymbol{J}$ to $\hat{\boldsymbol{A}}^*(\alpha) \odot \hat{\boldsymbol{A}}(\alpha)$ will give rise to a degree 1 deficiency; namely, the maximum DOF achievable of $2(M-1)$. According to Corollary 1 of [38], we know that a unique sparest representation $\boldsymbol{\rho}$ satisfies (20) does exist, if and if and only if

$$\|\boldsymbol{\rho}\|_0 < \frac{Spark(\boldsymbol{\Phi})}{2} \tag{38}$$

where $Spark(\boldsymbol{\Phi})$ denotes the smallest possible integer of columns of $\boldsymbol{\Phi}$ that are linearly dependent. With nonambiguity in the array structure, we can deduce that $Spark(\boldsymbol{\Phi}) = 2(M-1)+1$. Thus,

$$\|\boldsymbol{\rho}\|_0 \leq M - 1 \tag{39}$$

It is easy to obtain that the maximum separable signal number is $M-1$ by using the proposed method.

IV. SIMULATION RESULTS

In this section, a series of simulation results are presented to evaluate the effectiveness and superiority of the proposed method for joint DOD and DOA estimation in bistatic MIMO radar. In addition, the RD-MUSIC, RD-Capon and ESPRIT algorithms are adopted to compare with the proposed method. In the following simulations, a narrowband bistatic MIMO radar system with $M = 6$ transmit arrays and $N = 6$ receive arrays is considered, both transmit and receive arrays are half-wavelength inter-element spacing ULAs. The average root mean square error (RMSE) is used to evaluate the angle estimation performance, which is defined as

$$RMSE(\boldsymbol{\alpha}) = \sqrt{\frac{1}{KI}\sum_{i=1}^{I}\left\|\hat{\boldsymbol{\alpha}}_i - \boldsymbol{\alpha}\right\|^2} \tag{40}$$

$$RMSE(\boldsymbol{\beta}) = \sqrt{\frac{1}{KI}\sum_{i=1}^{I}\left\|\hat{\boldsymbol{\beta}}_i - \boldsymbol{\beta}\right\|^2} \tag{41}$$

where I denotes the number of the independent Monte Carlo trails. Unless explicitly stated, the RMSE curves presented in the follwing simulations are obtained by $I = 200$ independent trials. And, $\hat{\boldsymbol{\alpha}}_i$ and $\hat{\boldsymbol{\beta}}_i$ denote the estimated angular parameters of $\boldsymbol{\alpha}$ and $\boldsymbol{\beta}$ in the i-th trial, respectively. Assume that the DODs and DOAs of three imping uncorrelated narrowband far-field targets are $\boldsymbol{\alpha} = [15°, 25°, 35°]$ and $\boldsymbol{\beta} = [10°, 20°, 30°]$, respectively. Moreover, the predefined spatial sampling for all algorithms are from $-90°$ to $90°$ with

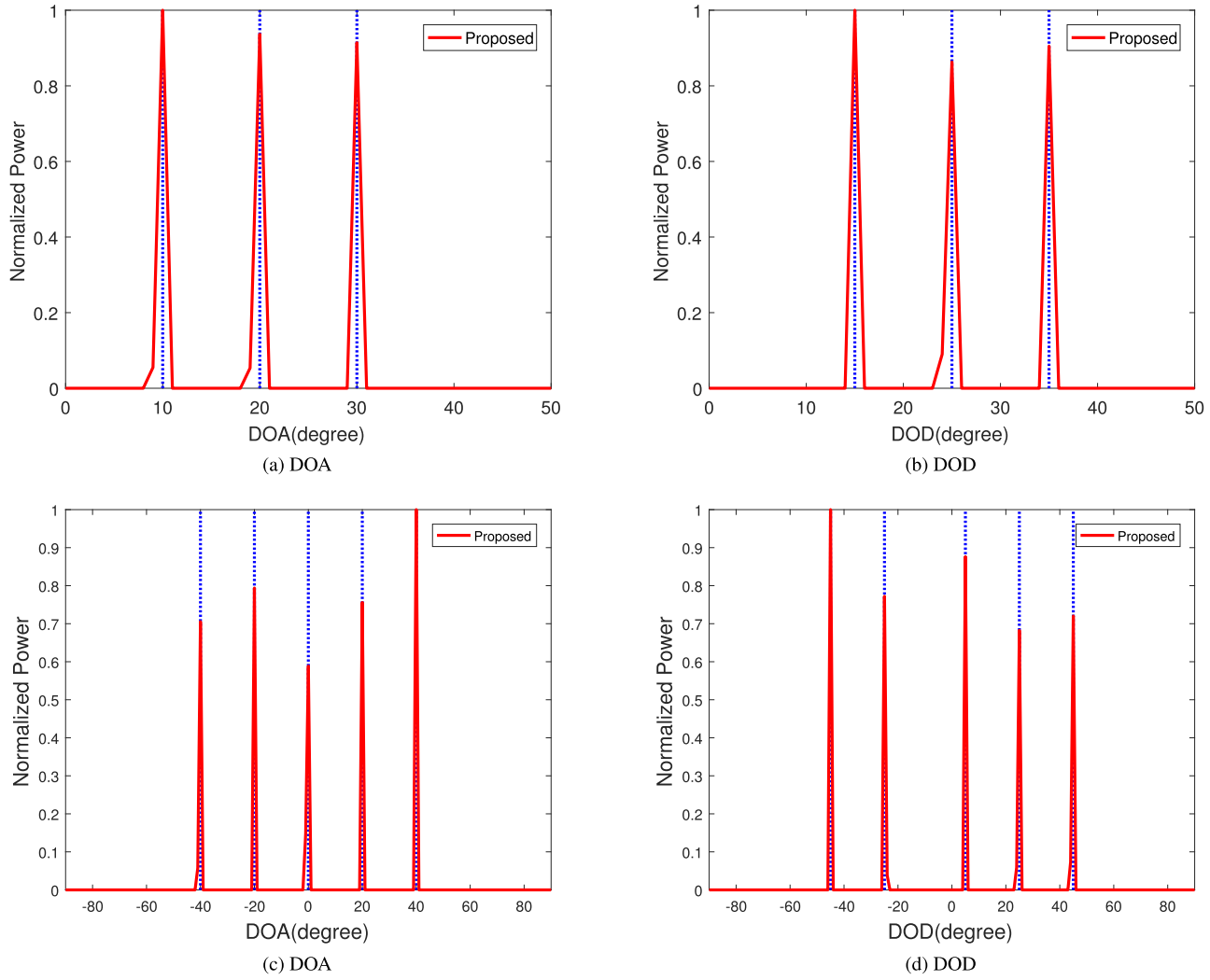

FIGURE 1. The DOA and DOD spatial spectrum by using the proposed sparsity based method.

the sampling interval being 1°, and the probability P_κ used in the proposed sparsity based method is set as 0.99999.

In the first experiment, we demonstrate the spatial spectrum estimation performance of the proposed algorithm, a total of 100 snapshots are used and SNR is set to 0dB. As illuminated in Fig. 1(a) and Fig. 1(b), we can find that the proposed sparsity based method can accuracy resolve the DODs and DOAs for three uncorrelated targets. As analysis in *Remark* 2, the maximum resolvable targets is 5 for $M = 6$ transmitters and $N = 6$ receivers. In order to further demonstrate the superiority of the proposed sparsity-based estimator, the spatial spectrum under the condition of the maximum resolvable targets is also provided. Assume that the DODs and DOAs of five imping uncorrelated narrowband far-field targets are $\boldsymbol{\alpha} = [-45°, -25°, 5°, 25°, 45°]$ and $\boldsymbol{\beta} = [-40°, -20°, 0°, 20°, 40°]$, respectively. Other simulation parameters are the same as Fig. 1(a) and Fig. 1(b). From Fig. 1(c) and Fig. 1(d), we can find that the proposed method can still provide a better spatial spectrum estimation under the condition of the maximum resolvable targets. And, we can see that the DODs and DOAs of the imping targets in Fig. 1(a) and Fig. 1(b) are in ascending order, namely $\alpha_1 < \alpha_2 < \alpha_3$ and $\beta_1 < \beta_2 < \beta_3$. The advantages of the this selection is that we can use the sparsity based estimator to realize the DODs and DOAs estimation without needing the angular parameter pairing, respectively. But, when the DODs and DOAs are out of order, the angular parameter pairing process is inevitable. This means that we can only use the sparse recovery method to estimate the DODs or DOAs based on the data model in (12) or (4). In the simulations of this paper, we omited the performance comparison between the proposed method with other methods when the DODs and DOAs are out of order. But after obtaing the estimated DODs or DOAs by using the proposed method, the detailed angular parameter pairing process is given in Appendix.

In the second experiment, the RMSE performance as a function of SNR and snapshots for the proposed method, RD-MUSIC algorithm, RD-Capon algorithm and ESPRIT

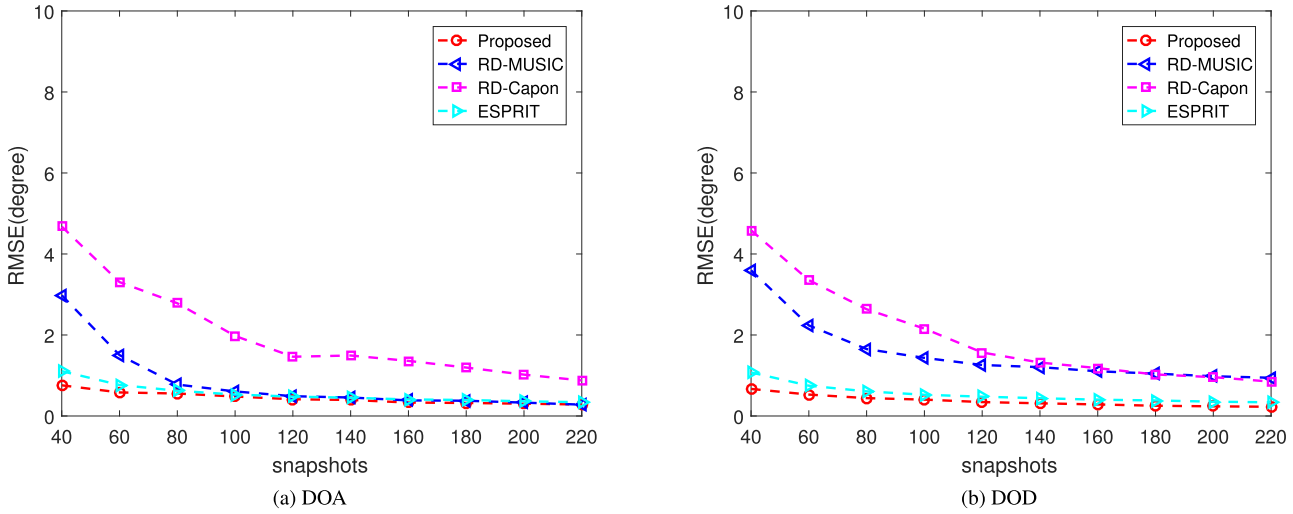

FIGURE 2. Performance comparison of different methods as a function of snapshots with SNR=0dB. (a-b) Root mean square error.

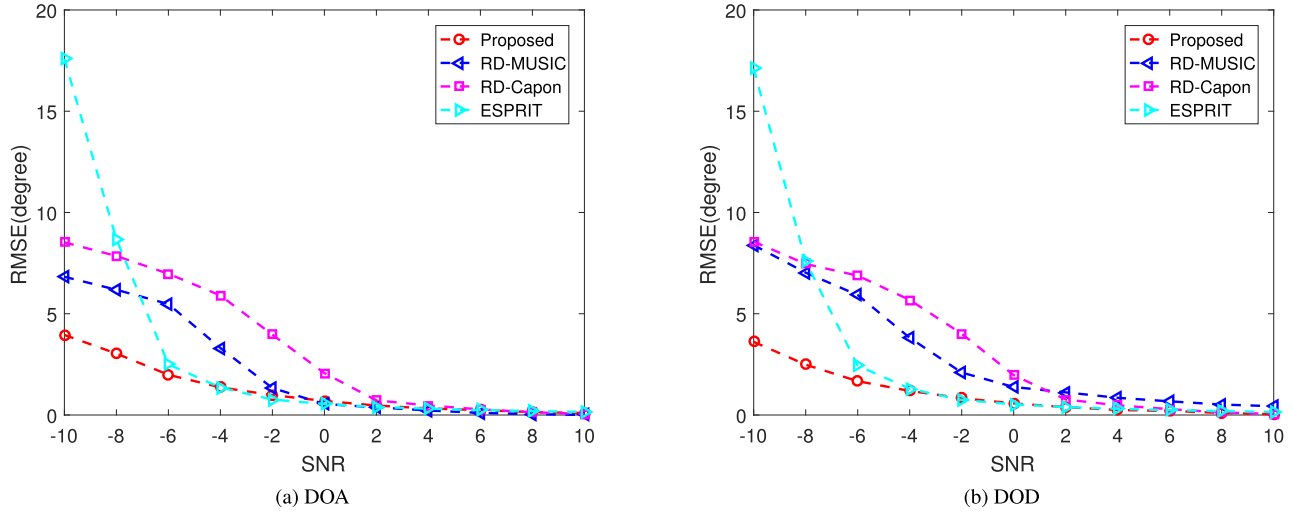

FIGURE 3. Performance comparison of different methods as a function of SNR with snapshots=100. (a-b) Root mean square error.

algorithm are demonstrated. As illuminated in Fig. 2, the number of snapshots increases from 40 to 220 with a step of 20 and the SNR is $0dB$ for all snapshots. It can be seen from Fig. 2 that the angular estimation precision of the proposed algorithm outperformances the RD-MUSIC algorithm, RD-Capon algorithm and ESPRIT algorithm with the number of the snapshots increases and the proposed method still work well when the available snapshots is relatively limited. In Fig. 3, the SNR increases from $-10dB$ to $10dB$ with a step of $2dB$ and the snapshots is fixed at 100. As shown in Fig. 3, the proposed method can provide lower SNR threshold with the SNR ranges from high noise region to low noise region. When the SNR is less than $-4dB$, the sparsity based method can still maintain a better angular estimaion precision while the other methods will produce relatively large error. From Fig. 2 and Fig. 3, it can be observed that the proposed sparsity based method can provide excellent estimation performance under the condition of the small snapshots and low SNR.

In the last experiment, we compare the angular super-resolution capabilities of the different algorithms mentioned above, the number of snapshots is fixed at 100 and the SNR is fixed at $0dB$. As illuminated in Fig. 4, the performance of RMSEs are compared. Two closely targets are considered, namely, the DOD and DOA of the first target is $(\alpha_1, \beta_1) = (15^\circ, 10^\circ)$,while the DOD and DOA of the second target is $(\alpha_2, \beta_2) = (15^\circ + \Delta\theta, 10^\circ + \Delta\theta)$. Where $\Delta\theta$ varies from 1° to 12° with a step size 1°. The result in Fig.4 shows that if the angular interval is small, the RMSE performance of the subspace estimators is very poor. But, for closely-spaced targets, the proposed method provides the minimum RMSE. For a more intuitive comparison, the spatial spectrum estimations are also provided when the angular separation is

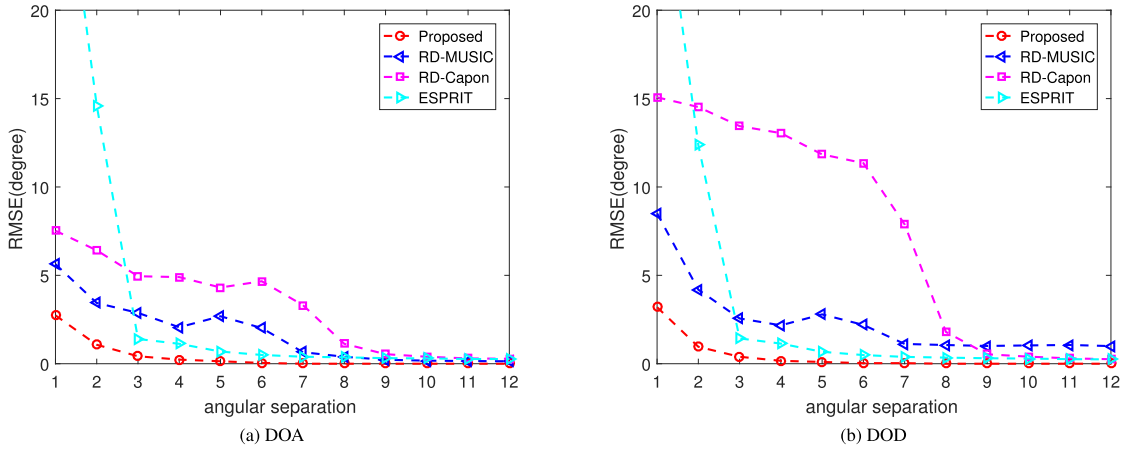

(a) DOA (b) DOD

FIGURE 4. Performance comparison of different methods as a function of angular interval with snapshots =100 and SNR=0dB. (a-b) Root mean square error.

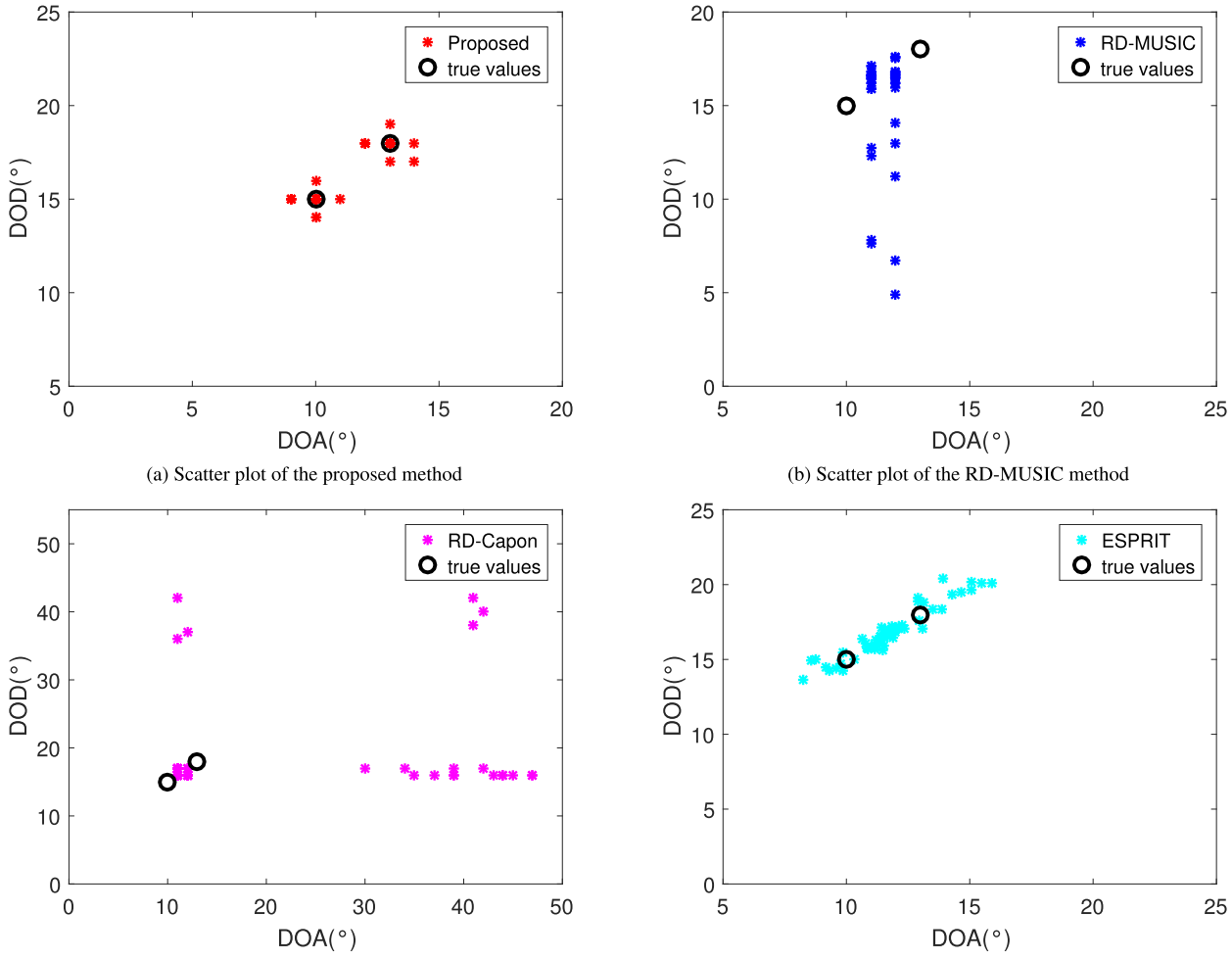

(a) Scatter plot of the proposed method

(b) Scatter plot of the RD-MUSIC method

(c) Scatter plot of the RD-Capon method

(d) Scatter plot of the ESPRIT method

FIGURE 5. Scattergram comparison of the proposed method, RD-MUSIC, RD-Capon and ESPRIT methods for two closely sources imping from $\alpha = [15°, 18°]$ and $\beta = [10°, 13°]$ with snapshots =100 and SNR=0dB.

small. Consider the DODs and DOAs of two closely spaced targets are $\boldsymbol{\alpha} = [15°, 18°]$ and $\boldsymbol{\beta} = [10°, 13°]$, respectively. Other simulation parameters are the same as Fig. 4. As illuminated in Fig. 5, the scattergram simulation results are obtained with the aid of 30 Monte Carlo trials, where the asterisks with different colors denote the estimates of

different angular parameters and the black circles denote the true angular parameters. It can be seen that the scattergram of the two closely spaced targets is relatively more concentrated by using the proposed method, which means that the proposed estimator can still provide superior estimation performance. On the other hand, the scattergrams in Fig. 5(b)-Fig. 5(d) are scattered. Thus, the simulation results in Fig. 4 and Fig. 5 demonstrate that the proposed sparse recovery method holds the best angle estimation performance for closely spaced targets.

V. CONCLUSION

A sparsity-based estimator has been proposed to deal with the DOD and DOA estimation in bistatic MIMO radars under the condition of low SNR region and/or small sample situation. And, the proposed new signal models can decouple the DOD and DOA in bistatic MIMO radars by stacking all the sampling data. The decoupling operation can avoid the construction of hugh dictionary matrix in the two dimension detection area. Furthermore, a selction matrix and whitening filter operation have been designed to mitigate the effect of the additive Gaussian noise and the perturbation errors. And, in order to guarantee the robust sparse recovery, an approach has been proposed for deriving the regularization parameter. Extensive simulation results demonstrate that the proposed sparsity recovery estimator can provide better angular estimation performance and higher spatial resolution than RD-MUSIC, RD-Capon and ESPRIT algorithms under the condition of low SNR region and/or small sample situation. And, in order to improve the adaptability of the proposed algorithm when the DODs and DOAs of the imping targets donot satisfy the ascending order or the descending order, the detailed angular parameter pairing process is also given. In the near future, we will focus on the gridless sparse recovery methods for the angular parameter estimation in bistatic MIMO radar system.

APPENDIX

ANGULAR PARAMETER PAIRED PROCESS

For disordered arrangement DODs and DOAs of the targets, we can firstly use the proposed sparse recovery algorithm to obtain the corresponding DODs or DOAs based (12) and (4), respectively. And, then the other angular parameters can be obtained by using the following process. Here, we derive the solution of DOAs when obtained the DODs by using the sparse recovery method and the same process for DODs can be adopted when obtained the DOAs by using the proposed method. Firstly, the sampling covariance matrix of (8) can be denoted as

$$\begin{aligned}\hat{\boldsymbol{R}}_{\bar{\boldsymbol{Y}}\bar{\boldsymbol{Y}}} &= \frac{1}{L}\bar{\boldsymbol{Y}}\bar{\boldsymbol{Y}}^H \\ &= (\boldsymbol{B}(\beta)\odot\boldsymbol{A}(\alpha))\hat{\boldsymbol{R}}_{\boldsymbol{\gamma}\boldsymbol{\gamma}}(\boldsymbol{B}(\beta)\odot\boldsymbol{A}(\alpha))^H + \hat{\boldsymbol{R}}_{\bar{\boldsymbol{w}}\bar{\boldsymbol{w}}} \end{aligned} \tag{42}$$

By performing eigenvalue decomposition on $\hat{\boldsymbol{R}}_{\bar{\boldsymbol{Y}}\bar{\boldsymbol{Y}}}$, we have

$$\hat{\boldsymbol{R}}_{\bar{\boldsymbol{Y}}\bar{\boldsymbol{Y}}} = [\boldsymbol{E}_{\boldsymbol{\gamma}}, \boldsymbol{E}_{\bar{\boldsymbol{w}}}]\boldsymbol{\Sigma}[\boldsymbol{E}_{\boldsymbol{\gamma}}, \boldsymbol{E}_{\bar{\boldsymbol{w}}}]^H \tag{43}$$

where the vectors in $\boldsymbol{E}_{\boldsymbol{\gamma}}$, associated with the K largest eigenvalues, span the signal subspace; while the vectors in $\boldsymbol{E}_{\bar{\boldsymbol{w}}}$, associated with the $MN - K$ small eigenvalues, span the noise subspace. $\boldsymbol{\Sigma}$ is a diagonal matrix whose elements are eigenvalues and arranged in descending order. Due to the orthogonality between the signal subspace and the noise subspace, we have

$$\left\|\boldsymbol{E}_{\bar{\boldsymbol{w}}}^H(\boldsymbol{b}(\beta)\odot\boldsymbol{a}(\alpha))\right\|^2 = 0 \tag{44}$$

By using the Kronecker product and vectorization operation, (44) can be rewritten as

$$\boldsymbol{V}(\alpha,\beta) = \left\|\boldsymbol{E}_{\bar{\boldsymbol{w}}}^H(\boldsymbol{b}(\beta)\odot\boldsymbol{a}(\alpha))\right\|^2 = \boldsymbol{b}(\beta)^H\boldsymbol{F}(\alpha)\boldsymbol{b}(\beta) \tag{45}$$

where $\boldsymbol{F}(\alpha) = (\boldsymbol{I}_M \otimes \boldsymbol{a}(\alpha))^H\boldsymbol{E}_{\bar{\boldsymbol{w}}}\boldsymbol{E}_{\bar{\boldsymbol{w}}}^H(\boldsymbol{I}_M \otimes \boldsymbol{a}(\alpha))$. It is can be found that the first element of the steering vector $\boldsymbol{b}(\beta)$ is 1. Thus, (44) can be further expressed as

$$\begin{aligned}&\min_{\alpha,\beta}\boldsymbol{b}(\beta)^H\boldsymbol{F}(\alpha)\boldsymbol{b}(\beta) \\ &s.t.\ \boldsymbol{e}_1^H\boldsymbol{b}(\beta) = 1\end{aligned} \tag{46}$$

Then, a new cost function for β can be constructed with the aid of the Lagrange theory, yielding

$$\boldsymbol{L}_{\alpha,\beta} = \boldsymbol{b}(\beta)^H\boldsymbol{F}(\alpha)\boldsymbol{b}(\beta) + \varsigma(\boldsymbol{e}_1^H\boldsymbol{b}(\beta) - 1) \tag{47}$$

where ς denotes the Lagrange multiplier. For fixed α, the derivative of the Lagrange function w.r.t β can be expressed as

$$\frac{\partial\boldsymbol{L}_{\alpha,\beta}}{\partial\boldsymbol{b}(\beta)} = 2\boldsymbol{F}(\alpha)\boldsymbol{b}(\beta) + \varsigma\boldsymbol{e}_1 = 0 \tag{48}$$

$$\hat{\boldsymbol{b}}(\beta) = \frac{\boldsymbol{F}^{-1}(\hat{\alpha})\boldsymbol{e}_1}{\boldsymbol{e}_1^H\boldsymbol{F}^{-1}(\hat{\alpha})\boldsymbol{e}_1} \tag{49}$$

By substituting the estimated $\hat{\alpha}$ using the sparse recovery method into (49), the corresponding estimated steering vector $\hat{\boldsymbol{b}}(\beta)$ can be obtained. Then, the shift invariance relationship between the first $N-1$ elements and last $N-1$ elements in $\hat{\boldsymbol{b}}(\beta)$ can be adopted to determine the final estimated $\hat{\boldsymbol{\beta}}$

$$\left[\hat{\boldsymbol{b}}(\beta)\right]_{1:N-1} exp(j\frac{2\pi}{\lambda}\sin(\beta_k)) = \left[\hat{\boldsymbol{b}}(\beta)\right]_{2:N} \tag{50}$$

$$\hat{\beta}_k = \arcsin(angle([\hat{\boldsymbol{b}}(\beta)]_{1:N-1}]^{\dagger}[\hat{\boldsymbol{b}}(\beta)]_{2:N})/\pi) \tag{51}$$

Thus, the DODs and DOAs can be automatically paired.

ACKNOWLEDGMENT

The authors acknowledge the interesting plenary talk about the bistatic MIMO radar with Prof. Lei Huang and Dr. Weize Sun. It inspired them to come up with the idea of using sparse recovery algorithm to bistatic MIMO radar.

REFERENCES

[1] E. Fishler, A. Haimovich, R. Blum, D. Chizhik, L. Cimini, and R. Valenzuela, "MIMO radar: An idea whose time has come," in *Proc. Proc. IEEE Radar Conf.*, Philadelphia, PA, USA, Apr. 2004, pp. 71–78.

[2] X. Wang, L. Wan, M. Huang, C. Shen, and K. Zhang, "Polarization channel estimation for circular and non-circular signals in massive MIMO systems," *IEEE J. Sel. Topics Signal Process.*, to be published. doi: 10.1109/JSTSP.2019.2925786.

[3] J. Xu, W.-Q. Wang, and R. Gui, "Computational efficient DOA, DOD, and Doppler estimation algorithm for MIMO radar," *IEEE Signal Process. Lett.*, vol. 26, no. 1, pp. 44–48, Jan. 2019.

[4] L. Mao, H. Li, and Q. Zhang, "Transmit design and DOA estimation for wideband MIMO system with colocated nested arrays," *Signal Process.*, vol. 152, pp. 63–68, Nov. 2018.

[5] L. Mao, H. Li, and Q. Zhang, "Transmit subaperturing for MIMO radars with nested arrays," *Signal Process.*, vol. 134, pp. 244–248, May 2017.

[6] M. Yang, L. Sun, X. Yuan, and B. Chen, "A new nested MIMO array with increased degrees of freedom and hole-free difference coarray," *IEEE Signal Process. Lett.*, vol. 25, no. 1, pp. 40–44, Jan. 2018.

[7] A. Liu, X. Zhang, Q. Yang, X. Wu, and W. Deng, "Combined root-MUSIC algorithms for multi-carrier MIMO radar with sparse uniform linear arrays," *IET Radar, Sonar Navigation*, vol. 13, no. 1, pp. 89–97, 2019.

[8] A. M. Haimovich, R. S. Blum, and L. J. Cimini, "MIMO radar with widely separated antennas," *IEEE Signal Process. Mag.*, vol. 25, no. 1, pp. 116–129, Jan. 2008.

[9] J. Li and P. Stoica, "MIMO radar with colocated antennas," *IEEE Signal Process. Mag.*, vol. 24, no. 5, pp. 106–114, Sep. 2007.

[10] H. Yan, J. Li , and G. Liao , "Multitarget identification and localization using bistatic MIMO radar systems," *EURASIP J. Adv. Signal Process.*, vol. 2008, Jan. 2008, Art. no. 48.

[11] X. Zhang, L. Xu, L. Xu, and D. Z. Xu, "Direction of departure (DOD) and direction of arrival (DOA) estimation in MIMO radar with reduced-dimension MUSIC," *IEEE Commun. Lett.*, vol. 14, no. 12, pp. 1161–1163, Dec. 2010.

[12] X. Zhang and D. Xu, "Angle estimation in MIMO radar using reduced-dimension capon," *Electron. Lett.*, vol. 46, no. 12, pp. 860–861, Jul. 2010.

[13] C. Duofang, C. Baixiao, and Q. Guodong, "Angle estimation using ESPRIT in MIMO radar," *Electron. Lett.*, vol. 44, no. 12, pp. 770–771, Jun. 2008.

[14] C. Jinli, G. Hong, and S. Weimin, "Angle estimation using ESPRIT without pairing in MIMO radar," *Electron. Lett.*, vol. 44, no. 24, pp. 1422–1423, Nov. 2008.

[15] M. L. Bencheikh, Y. Wang, and H. He, "Polynomial root finding technique for joint DOA DOD estimation in bistatic MIMO radar," *Signal Process.*, vol. 90, pp. 2723–2730, Sep. 2010.

[16] Y. Cheng, R. Yu, H. Gu, and W. Su, "Multi-SVD based subspace estimation to improve angle estimation accuracy in bistatic MIMO radar," *Signal Process.*, vol. 7, pp. 2003–2009, Jul. 2013.

[17] B. Tang, J. Tang, Y. Zhang, and Z. D. Zheng, "Maximum likelihood estimation of DOD and DOA for bistatic MIMO radar," *Signal Process.*, vol. 5, pp. 1349–1357, May 2013.

[18] F. K. W. Chan, H. C. So, L. Huang, and L.-T. Huang, "Under-determined direction-of-departure and direction-of-arrival estimation in bistatic multiple-input multiple-output radar," *Signal Process.*, vol. 104, pp. 284–290, Nov. 2014.

[19] T.-Q. Xia, "Joint diagonalization based DOD and DOA estimation for bistatic MIMO radar," *Signal Process.*, vol. 108, pp. 159–166, Mar. 2015.

[20] T.-Q. Xia, "Joint diagonalization based 2D-DOD and 2D-DOA estimation for bistatic MIMO radar," *Signal Process.*, vol. 116, pp. 7–12, Nov. 2015.

[21] X. Wang, W. Wang, J. Liu, Q. Liu, and B. Wang, "Tensor-based real-valued subspace approach for angle estimation in bistatic MIMO radar with unknown mutual coupling," *Signal Process.*, vol. 116, pp. 152–158, Nov. 2015.

[22] C. Cai, F. Wen, and D. Huang, "New approach to angle estimation for bistatic MIMO radar with unknown spatially colored noise," *IEEE Access*, vol. 6, pp. 24249–24255, 2018.

[23] L.-T. Huang, A. L. F. de Almeida, and H. C. So, "Target estimation in bistatic MIMO radar via tensor completion," *Signal Process.*, vol. 120, pp. 654–659, Mar. 2016.

[24] J. Liu, W. Zhou, F. H. Juwono, and D. Huang, "Reweighted smoothed ℓ_0-norm based DOA estimation for MIMO radar," *Signal Process.*, vol. 137, pp. 44–51, Aug. 2017.

[25] X. Wang, W. Wang, J. Liu, X. Li, and J. Wang, "A sparse representation scheme for angle estimation in monostatic MIMO radar," *Signal Process.*, vol. 104, pp. 258–263, Nov. 2014.

[26] X. Wang, L. Wang, X. Li, and G. Bi, "Nuclear norm minimization framework for DOA estimation in MIMO radar," *Signal Process.*, vol. 135, pp. 147–152, Jun. 2017.

[27] J. Liu, W. Zhou, and X. Wang, "Fourth-order cumulants-based sparse representation approach for DOA estimation in MIMO radar with unknown mutual coupling," *Signal Process.*, vol. 128, pp. 123–130, Nov. 2016.

[28] H. Wang, L. Wan, M. Dong, K. Ota, and X. Wang, "Assistant vehicle localization based on three collaborative base stations via SBL-based robust DOA estimation," *IEEE Internet Things J.*, vol. 6, no. 3, pp. 5766–5777, Jun. 2019.

[29] F. Dong, C. Shen, K. Zhang, and H. Wang, "Real-valued sparse DOA estimation for MIMO array system under unknown nonuniform noise," *IEEE Access*, vol. 6, pp. 52218–52226, 2018.

[30] D. Malioutov, M. Cetin, and A. S. Willsky, "A sparse signal reconstruction perspective for source localization with sensor arrays," *IEEE Trans. Signal Process.*, vol. 53, no. 8, pp. 3010–3022, Aug. 2005.

[31] Z.-M. Liu, Z.-T. Huang, and Y.-Y. Zhou, "Sparsity-inducing direction finding for narrowband and wideband signals based on array covariance vectors," *IEEE Trans. Wireless Commun.*, vol. 12, no. 8, pp. 1–12, Aug. 2013.

[32] M. Huang, L. Huang, C. Guo, P. Zhang, J. Zhang, and L.-L. Yang, "Carrier frequency offset estimation in uplink OFDMA systems: An approach relying on sparse recovery," *IEEE Trans. Veh. Technol.*, vol. 66, no. 10, pp. 9592–9597, Oct. 2017.

[33] X. Xu, X. Wei, and Z. Ye, "DOA estimation based on sparse signal recovery utilizing weighted ℓ_1-norm penalty," *IEEE Signal Process. Lett.*, vol. 19, no. 3, pp. 155–158, Mar. 2012.

[34] B. D. Rao, K. Engan, S. F. Cotter, J. Palmer, and K. Kreutz-Delgado, "Subset selection in noise based on diversity measure minimization," *IEEE Trans. Signal Process.*, vol. 51, no. 3, pp. 760–770, Mar. 2003.

[35] S. Boyd and L. Vandenberghe, *Convex Optimization*. London, U.K.: Cambridge Univ. Press, 2004.

[36] M. Grant and S. Boyd. (2012). *CVX: MATLAB Software for Disciplined Convex Programming, Version 1.22*. [Online]. Available: http://cvxr.com/cvx

[37] J. Shi, G. Hu, X. Zhang, F. Sun, and H. Zhou, "Sparsity-based two-dimensional DOA estimation for coprime array: From sum–difference coarray viewpoint," *IEEE Trans. Signal Process.*, vol. 65, no. 21, pp. 5591–5604, Nov. 2017.

[38] D. L. Donoho and M. Elad, "Optimally sparse representation in general (nonorthogonal) dictionaries via ℓ^1 minimization," *Proc. Nat. Acad. Sci. USA*, vol. 100, no. 5, pp. 2197–2202, 2003.

QIANPENG XIE was born in Henan, China, in 1991. He received the B.S. and M.S. degrees from the National University of Defense Technology, Hefei, China, in 2014 and 2016, respectively, where he is currently pursuing the Ph.D. degree. His research interests include array signal processing, radar signal processing, and electromagnetic environment effects.

XIAOYI PAN was born in Anhui, China, in 1986. He received the M.S. and Ph.D. degrees in information and communication engineering from the National University of Defense Technology, Changsha, China, in 2009 and 2014, respectively.

He is currently a Lecturer with the National University of Defense Technology. His research interests include inverse synthetic aperture radar imaging, feature extraction, and electromagnetic environment effects.

MIN HUANG received the B.S. and Ph.D. degrees in electrical communication from Xidian University, China, in 2008 and 2015, respectively. He is currently a Postdoctoral Fellow with the Shenzhen Key Laboratory of Advanced Navigation Techniques, Shenzhen University. His research interests include channel estimation, OFDM signal detection, and compressive sensing algorithms.

JIYUAN CHEN was born in Yunnan, China, in 1994. He received the bachelor's degree in electronic engineering from the National University of Defense Technology, Changsha, China, in 2017, where he is currently pursuing the master's degree. His research interests include inverse synthetic aperture radar imaging and electromagnetic environment effects.

SHUNPING XIAO was born in Jiangxi, China, in 1964. He received the B.S. and Ph.D. degrees in electronic engineering from the National University of Defense Technology (NUDT), Changsha, China, in 1986 and 1995, respectively, where he is currently a Professor.

His research interests include radar target recognition and radar signal processing. He is also a Senior Member of CIE.